The 2010 IEEE/RSJ International Conference on
Intelligent Robots and Systems
October 18-22, 2010, Taipei, Taiwan

The DLR Touch Sensor I: A Flexible Tactile Sensor for Robotic Hands based on a Crossed-Wire Approach

M.W. Strohmayr, H.P. Saal, A.H. Potdar and P. van der Smagt

Abstract— **One of the main challenges in service robotics is to equip dexterous robotic hands with sensitive tactile sensors in order to cope with the inherent problems posed by unknown and unstructured environments. As the increasing mechatronic integration of complex robotic hands leaves little additional space for proprioceptive sensors, exteroceptive tactile sensors become more and more important. We present a novel tactile sensor design, based on piezo-resistive soft material and a crossed-wire approach. We present the development of a first prototype and its evaluation in various classification tasks, showing promising results.**

I. Introduction

Today, an increasing number of robotic devices is developed to support humans in a variety of everyday tasks[29], [21]. In contrast to the well-defined conditions in industrial production lines, the unstructured nature of human environments is particularly challenging for robotic devices.

It has been shown that humans make extensive use of their sense of touch when grasping and manipulating objects, and that any impairments can severely affect their dexterity. Robots face similar problems, as pre-defined object models or visual sensor data might not provide enough information for setting grip forces correctly or fine-grained handling of objects. Especially the manipulation of small objects designed for human hands is a challenging problem: Safe gripping and manipulation of a shirt button or a match still is an almost unsurmountable challenge for robotic manipulators. Sophisticated tactile sensors are needed in order to tackle such problems.

Therefore, there is an increasing need for such sensor systems, and a variety of different approaches has been proposed over the last years. One of the problems in the widespread adoption of tactile sensors is difficult integration with existing robotic hardware, mainly robotic hands. Often, these manipulators offer only limited or no space for additional sensor processing equipment or bulky rigid parts. Ideally, touch sensors should consist of a skin-like soft and flexible material providing a coating to the robotic fingers devoid of rigid or bulky parts.

In this paper, we present the development and a first prototype of the DLR Touch Sensor I. It is based on a novel crossed-wire design, compliant, and robust.

The paper is structured as follows: In Section II, we review different approaches to tactile sensing and current designs of hands equipped with tactile sensors. Section III then introduces the DLR crossed-wire approach, the materials used, and the manufacturing of the prototype sensors. In Section IV the sensor patches are evaluated with respect to their behaviour and capabilities for object shape classification.

DLR - German Aerospace Center, Institute of Robotics and Mechatronics, Germany. Contact: michael.strohmayr@dlr.de. This work is supported by the FP6 EU project SENSOPAC (028056)

II. Tactile sensors

A. Overview

This section gives a brief overview of the state of the art in tactile sensor development. According to [23] a tactile sensor is defined as "a device or system that can measure a given property of an object or contact event through physical contact between the sensor and the object". There are two categories of tactile sensors: Intrinsic or proprioceptive and extrinsic or exteroceptive tactile sensors [25]. Proprioceptive sensors are mostly located in or at rigid supporting structural elements, and do not directly measure properties of contacting objects but rather gather indirect information on impacting forces. This allows for the calculation of information regarding contact properties. Exteroceptive sensors are in principle capable of measuring contact location, pressure distribution, and shear forces. Most often arrays with active or passive taxel sampling are used. An overview of the different transduction principles applied in tactile sensors is given in [23], [6]. Extensive research has been conducted for transduction methods based on the measurement of various quantities and effects. Table I exemplarily lists tactile sensor setups based on the most commonly applied transduction principles. Up to now, there is no consensus as to which is the optimal transduction principle for tactile sensing for robotic hands. As recommended in [26], piezo-resistivity is likely to be one of the most promising transduction principles for the application in tactile sensors for robotic hands. Additionally, it allows for designs made entirely out of flexible material and is therefore a promising candidate for the design of flexible coatings.

Transduction principle	Setup	Reference
Resistance	array	[32]
Capacitive	single cell	[19]
Piezo-electric	array	[20]
Magnetic	array	[4]
Optical	array	[16]
Ultrasonic	single cell	[1]

TABLE I
Transduction principles and examples

978-1-4244-6676-4/10/$25.00 ©2010 IEEE

Name	extr. tact. sensor	transduct. principle	No. of Taxels	min. spacial resolution	Reference
Gifu Hand II	array	conductivity	624	$4-6$ mm	[18]
Anthropomorphic hand (Karlsruhe)	array	conductivity	$7x4$ taxel/patch	n/a	[10]
Multi-fingered hand (Univ. of Tokyo)	surface	conductivity	center position	n/a	[11]
Multi-fingered hand (Sony)	array	capacitive	86 taxel/ fingertip	3 mm	[30]

TABLE II

DEXTEROUS ROBOTIC WITH TACTILE SENSORS

B. Exteroceptive tactile sensors for robotic hands

There is a multitude of robotic hands being developed by many groups. We present a small subset which is equipped with tactile sensors in Table II.

Recent advances in robotic hand development allow for increasingly sophisticated tasks to be conducted by robotic hands. Integration of tactile sensors into robotic hands results in additional requirements: To extend the dexterity to rolling objects between the fingertips, mostly cylindrical, spherical, or 3D-free-form surfaces are applied at the fingertips. Tactile sensors dedicated to the application on those fingertips need to be deformable or conformable to the shape of the fingertips to support the desired dexterity.

There is an increasing number of promising approaches towards the integration of tactile sensors into dexterous manipulation scenarios. However, up to now there is no commercially available tactile sensor system available that is mountable on 3-D free-form surfaces like robotic fingertips and, at the same time, provides high mechanical compliance to support the dexterous capabilities of the robotic hand.

Our touch sensor is developed with the aim to be eventually mounted on the DLR Hand II. This hand is based on four identical fingers. Each finger is equipped with four joints, with the last two joints mechanically coupled. The intrinsic sensors of DLR Hand II provide information about motor-positions, joint-angles and joint-torques as well as temperature. In addition, the fingertips are equipped with custom-made six-DoF force-torque sensors based on strain gauges [3]. With this sensor setup a glass of tea can be prepared and served [7].

The current version of DLR Hand II is not equipped with exteroceptive sensors, which limits the dexterity of the hand, for example when manipulating small objects. Therefore we focus our development on flexible sensors that could provide a suitable tactile coating for the hand's outer surface (fingers, especially the tips, and palm).

III. DESIGN

In this section the working principle of the first generation of the DLR touch sensor is described.

A. Crossed-wire design

The DLR crossed-wire approach is based on piezo-resistivity as transduction effect. With a focus on easy and low cost manfuacture, mechanically simple designs for the test patches were preferred. Therefore, we focused on "classical" array setups. The first approach is based on injection-molded patches with cast in wires.

As shown in Fig. 1, the wires are arranged in two different layers. Those layers are separated by the piezo-resistive matrix, which forms sensitive areas at each crossing point of two wires. One of the advantages of such a design is that the number of connecting cables does not increase linearly with the number of taxels. Due to space limitations, processing of the tactile information cannot happen directly on the hand and keeping the number of connections manageable while still providing a high spatial resolution is a key requirement.

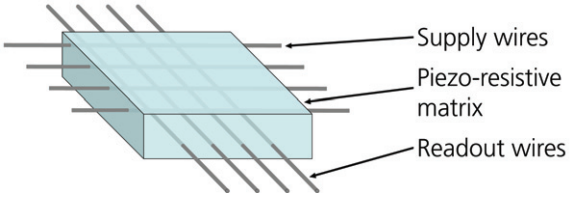

Fig. 1. Setup with different layers of wires

B. Materials

The first challenge was the production of a thermoplastic elastomer exhibiting piezo-resistivity, so we could use this material in injection molding. In piezo-resistive materials the resistivity depends on the concentration of conductive filler particles, geometric form, and distribution. A piezo-resistive behavior can be observed if a non-conducting material is endowed with conductive particles.

Recently many experimental studies have been conducted aiming towards the theoretical description of the effects that are observable in different polymers filled with conductive particles [17], [24], [22], [27], [28], [33]. An overview of the work is given in [12]. A short insight into the application of conductive polymers as pressure sensors is outlined in [13].

For the application of a piezo-resistive material as pressure sensor the desired material properties can be achieved by the optimal selection of the basis material and the adjustment of the tunable properties with a focus to the desired mechanical and electrical properties.

As no commercially available granulates with the desired piezo-resistive profile existed, we ran several experiments to determine materials suitable for blending in order to achieve the required properties: Easy miscibility with conductive fillers, tuneable mechanical properties and processability in injection molding machines.

We focused on ultra-soft Poly[styrene-b-(ethylene-co-butylene)-b-styrene] (SEBS) polymers in order to make the resulting patches compliant and flexible. Blending these materials with pre-filled polymers of high conductivity did not prove successful. We also discarded pure graphite as a filler material. However, using carbon black as a filler material, we were able to produce granulate with the desired piezo-resistive properties. For these mixtures we used Kraiburg Thermolast TF0STL (0 Shore A) [31] and Cabot Vulcan

XC72 (carbon black) [5].

For the blending of the polymer and the carbon black, we used a twin-screw extruder. The self-compounded ultrasoft polymers was granulated by cooling it with liquid nitrogen. The resulting granules were then processed by the injection molding machine.

C. Manufacture

For the injection molding a Battenfeld MicroSystem 50 injection molding machine was used [8]. This machine is designed for the processing of small volumes and molds in [mm] scale.

We produced various test patches with different filler ratios on the injection molding machine. The patches are equipped with cast-in steel wires, see Fig. 2.

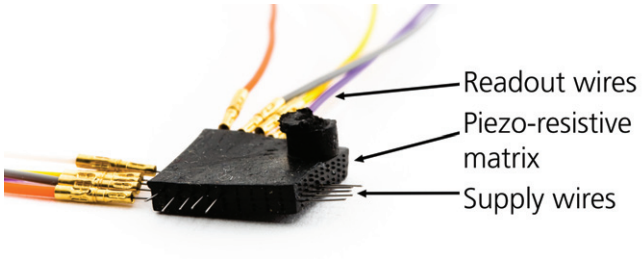

Fig. 2. 11 mm x 11 mm SEBS testpatch, contacting wires

We found that an estimated filler ratio of about 30 w/w showed the best piezo-resistive effect. Manual indentation of the patches resulted in measurable changes in resistance ranging from 3 MΩ to 100 kΩ.

IV. Evaluation

In this section different piezo-resistive materials and their applicability in tactile sensor setups are investigated. We first described the mechanical testbed that we used in Section IV-A. Then, we present the results of simple indentation tests examining the piezo-resistive behaviour of the sensor patches in Section IV-B. Finally, we present object shape classification results in Section IV-C and multi-point discrimination in Section IV-D.

A. Mechanical testbed

The testbed depicted in Fig. 3 is designed to conduct indentation tests for evaluating the manufactured sensor patches.

Another goal in the development of the testbed was maximum flexibility and accuracy at reasonable cost. The testbed consists of a frame to support the test patch and the DLR linear drive cylinder [2]. The drive cylinder is equipped with position and force sensors and is able to provide up to 300 N at a spacial resolution of 2μm. To enable horizontal movement of the tested specimen a x/y-platform with a spacial resolution of 1μm is applied. To measure the forces exerted on the patch, an optical force torque sensor from SpaceControl [9] with a force-resolution of 20 mN is applied.

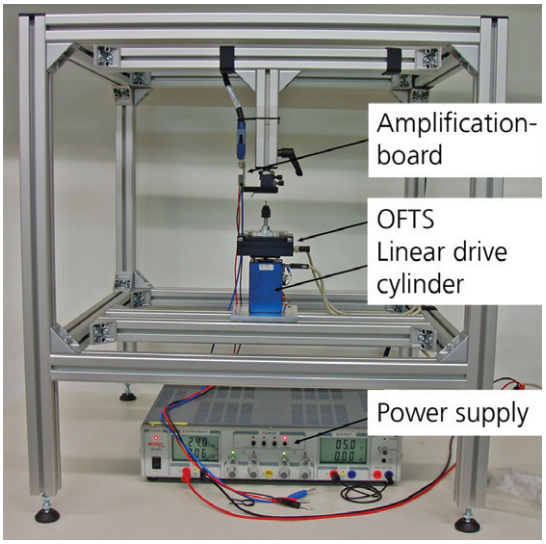

Fig. 3. The DLR skin testbed

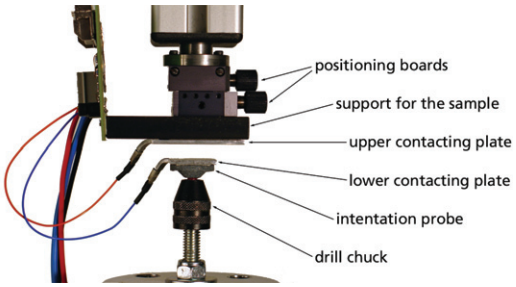

Fig. 4. Details of the testbed

B. Indentation tests

1) Experiments and results: To evaluate the quality of the piezo-resistive effect and to determine whether the proposed sensor setup is applicable in robotic hands the manufactured sensor patches are analysed on the testbed. For these tests the patches are covered with an electrically insulating foil to ensure the sole measurement of the effects within the patch.

A square aluminum plate with a surface of 400 mm^2 is used as indentation probe, see Fig. 4. Thus, the probe covers the entire patch avoiding possible influences of a varying indentation location. For the readout of the resistance two crossing, cast-in wires are connected to a pre-amplification board where the resulting current is measured over a reference resistor.

The patches are fixed on the testbed and loaded with a trapezoidal indentation path. The linear motor is operated in position control mode and commanded to indent the patch at a certain speed, then stop and maintain a pre-set indentation depth for a defined period of time and then to release the patch, again with a defined velocity.

For every mixing ratio a patch is tested applying:

- indentation depth 1 mm
- indentation speed $100\frac{\mu\text{m}}{\text{s}}$ to $1000\frac{\mu\text{m}}{\text{s}}$
- maximum indentation force 55 N
- hold time 10 s

- release speed $100\frac{\mu m}{s}$ to $1000\frac{\mu m}{s}$

For the evaluation of the piezo-resistive effect, time, commanded indentation depth, actual indentation depth, force in z-axis and measured voltage is recorded and stored.

The prototype patches clearly show a piezo-resistive effect. But during the test on the testbed the patches also showed an unexpected behavior. If the load is increased faster than $500\frac{\mu m}{s}$ the measured voltage shows an unexpected dip. Contrary to the expected behavior an initial increase of the resistance is observable, see Fig. 5.

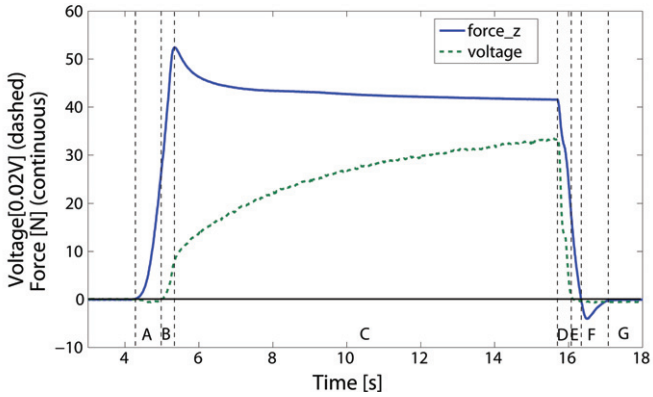

Fig. 5. Piezo-resistive behavior - SEBS

In region A the force increases exponentially due to the indentation, while the measured voltage shows an unexpected behavior, it decreases (i.e., the resistance increases). Within region B the patch exhibits the expected piezo-resistive behavior, as the voltage increases exponentially while the force increases linearly. During the pre-set hold time (region C) the curve of the force shows a typical course for highly compliant materials. While the given position is maintained the material shuns from the load and the force slowly decreases. Due to the applied force an increasing amount of conductive pathways is formed within the piezo-resistive matrix material. Therefore, the voltage slowly increases towards a saturation. In region D the voltage decreases proportional to the force. While the force decreases further in region E, the voltage converges to a constant value slightly below its initial value. Within region F a negative force is observable, as the linear drive cylinder pulls the patch which adheres to the upper support of the specimen, the measured voltage decreases only slightly. At the end of the indentation test, in region G, the force reaches its initial value and the voltage maintains a value slightly below its initial value. Additional experiments revealed a velocity-dependent behavior of the test-patch. The above described trapezoid indentation path was applied to the patch with indentation and release velocities of, $0.1\frac{mm}{s}$, $1\frac{mm}{s}$, and $10\frac{mm}{s}$. Figure 6 shows the velocity-dependent response of the test-patch.

If pressure is applied to the patch, the matrix material shuns from the load. Due to the difference in elasticity a relative motion between wires and sensor matrix is induced. Fast indentation of the patches results in increasing resistivity. This effect might be caused by an altering transfer resistance between matrix and cast-in metal wires. When the matrix material is deformed quickly, it partly lifts off from the metal wires and the transfer resistance temporarily increases. Possibly the slow indentation allows the material to maintain sliding contact to the wires, which has only minor influence to the transition resistivity. To show the causative effects the behavior of the SEBS patches with cast-in steel wires is simulated using ANSYS [14].

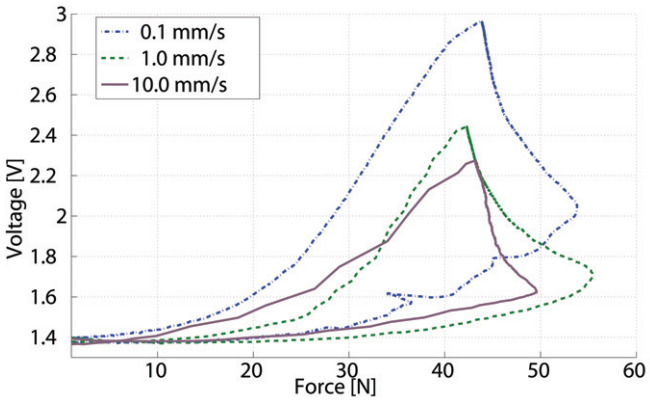

Fig. 6. Velocity dependent response

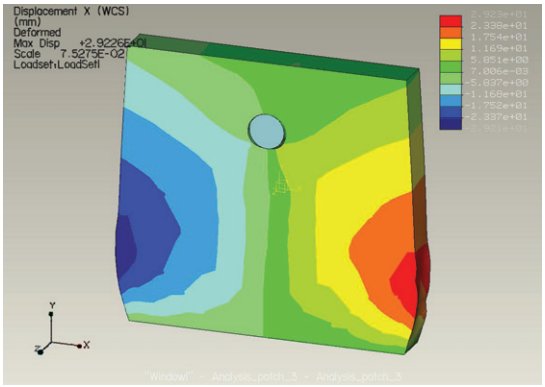

Fig. 7. Simulation of the cast-in wire

2) Simulations: To minimize computational effort, a thin slice of matrix material is calculated in 2D, see Fig. 7. Within the matrix material a hole is defined containing a metal cylinder representing the wire. The connection between the cylinder and the surrounding matrix is defined as loose. The following parameters are applied: For the wire the material parameters of "AL2014" are used. It exhibits an isotropic density of $2.79355 \cdot 10^{-3}\ \frac{g}{mm^3}$, a Young's Modulus of $7.30844 \cdot 10^{10}\ \frac{g}{mm \cdot s^2}$, and a Poisson's Ratio of 0.33. For the compliant matrix material "Silastic" is applied, with an isotropic density of $0.2 \cdot 10^{-3}\ \frac{g}{mm^3}$; an idealized Young's Modulus of $2.05 \cdot 10^{6}\ \frac{g}{mm \cdot s^2}$; and a Poisson's Ratio of 0.29. The top plane of the modeled slice of the compliant matrix material is laminarly loaded with a load in the y-axis. While the bottom plane is fixed. To allow the material to shun from the load the side planes are defined as freely deformable. Then the model is statically loaded with 10 N

and the resulting displacement in 2D is shown in different colors.

Due to the applied force the matrix material bulges to the sides. In addition, the highly compliant matrix material shuns from the load and lifts off the wire in the x-axis, see Fig. 7.

Complemetary to the simulations, the sensor patches were examined using scanning electron microscopy (SEM), see Fig. 8. The examination with the SEM reveals the most

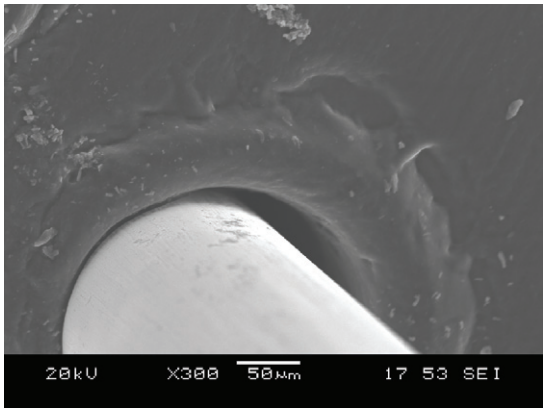

Fig. 8. SEM of the wire cast into SEBS

likely reason for the observed phenomena: The low adhesion between the SEBS matrix and the cast-in steel wires.

C. Object shape classification

To be able to apply the DLR touch sensor as an exteroceptive sensor for the DLR-Hand, not only the piezo-resistive characteristics but also the discrimination of different indentation probes at different indentation depth and forces is relevant, highlighting fine-grained tactile capabilities.

In order to test this, different indentation probes (cylindrical, spherical, parabolic and a spezialised 1-4 point probe) are applied to the touch sensors, see Fig. 9.

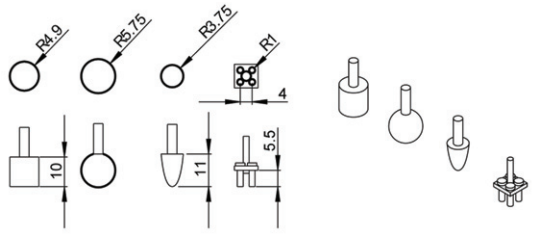

Fig. 9. Geometry of the indentors, all values in [mm]

The prototype sensor patches are attached to the testbed using double-sided duct tape. The test patch is then loaded according to a defined indentation path. Sequentially different areas of the sensor patch are indented with the probe. Therefore the support of the specimen can be manually deviated in μm steps. Thus the entire sensitive area of the test patch is evaluated with one indentation probe. Subsequently the whole test is repeated applying different indentation probes. Figure 10 shows the different indentors and the response of the sensor patch.

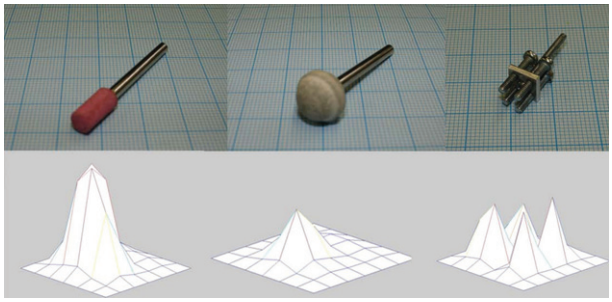

Fig. 10. Indentors, patch output

The first set of tests revealed promising characteristics of the SEBS thermoplastic patches. With the realised spatial resolution of less than one mm the different indentation probes can easily be discriminated by eye. To test the classification performance of the sensor patches a simple 2-layer feed forward neural network (Fig. 11) is applied for the interpretation of the values from the sensor readout system. A single neuron which makes up the network can be described by the following equation 1:

$$y_j = f_j(\sum w_{ij} x_i + \theta_j) \tag{1}$$

were y_j is the output of neuron, x_i are the inputs to the neuron, f_j is the activation function, w_{ij} are the weights between the inputs and the neuron and θ_j is the bias for the output neuron. The applied neural network contains 4 output neurons, each for one indentor geometry. The above

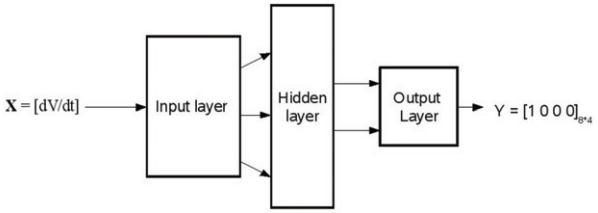

Fig. 11. 2-layer feedforward neural network

described indentors are used to apply force to the sensor patch with the goal of correct classification of the indentor. On the testbed defined forces ranging from 0 N to 5 N have been cyclicly applied to the patches, and the output of the sensor patch as well as the indentation position and force have been recorded. Subsequently, the neural network was trained using two datasets for each indentor containing 208 datapoints for each taxel. In the following, a sequence of two unknown sets for the same indentor are presented to the neural network. This procedure is repeated for the different indentor types (spherical, cylindrical, paraboloid and a variable 1-4 point indentor). The rate of change of the output voltage for the given indentation produced the features, which are used as training input for the neural network, see Fig. 12.

The conducted experiments proved the ability of the neural network to classify the 8 sets correctly, if the sensor is loaded with the specified indentation sequence. The first output

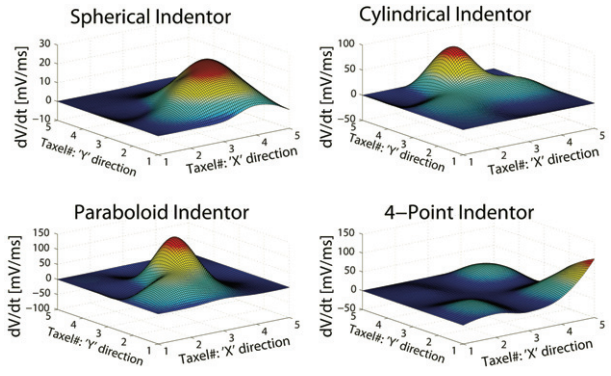

Fig. 12. Rate of change of the output signals (Voltages) as features for the classification of different indentors

neuron switched to 1 for the first 2 datasets for the spherical indentor followed by the successive switching of the second, third and fourth output neuron to 1 when indented with the cylindrical, paraboloid and variable $1-4$ point indentor. The shape (i.e. the geometry) of the indentor was correctly classified using simple neural networks.

D. Multi-point orientation classification

To test the ability of the sensor patch to discriminate between multiple contact indentations of [mm]-scale objects at [mm]-scale deviation the classification of six different indentation scenarios was investigated.

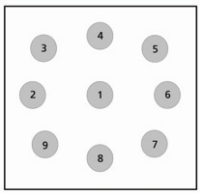

Fig. 13. Sensor Patch: Postions of Indentations

Six different training classes are obtained from the sensor readout applying the following indentations (Fig. 13):

1) Spherical indentor: Force application on a force dependent circular area (Position 1).
2) Cylinder indentor: Force application on a circular area (Position 1).
3) Vertical indentation: Force applied on two points (Position 4 and 8) on the sensor patch which are placed vertically opposite to each other (4 mm spacing).
4) Horizontal indentation : Force applied on two points (Position 2 and 6) on the sensor patch which are placed vertically opposite to each other (4 mm spacing).
5) Diagonal indentation (URLL): Force applied on two points (Position 5 and 9) located on upper right and lower left ends of the diagonal (6 mm spacing).
6) Diagonal indentation (ULLR): Force applied on two points (Position 3 and 7) located on upper left and lower right ends of the diagonal (6 mm spacing).

Five datasets for each indentations were recorded over a time of 5 minutes. To enlarge the information content of the input space, different training sets were generated with two consecutive datasets and a combination of the first and the last dataset. A neural network was trained using the training sets and subsequently tested applying an independent test dataset unknown to the network. The independent test dataset included data for all the indentation positions mentioned above.

The table in Fig. 14 shows that the training set combination of the first and last data sets gives the minimum error of approximately 5% for the classification of the different indentation positions as compared to the other training set combinations. Reduced classification accuracy was obtained with the training sets recorded initially and tested with datasets obtained later w.r.t. time. This is due to the fact

	Test1	Test2	Test3	Test4	Test5
Train_[12]	0.0003	0.0001	0.2255	0.1617	0.2812
Train_[23]	0.1729	0.0002	0.0004	0.0323	0.0563
Train_[34]	0.2599	0.2135	0.0003	0.0002	0.0425
Train_[45]	0.3460	0.1273	0.0567	0.0002	0.0002
Train_[51]	0.0003	0.0473	0.0498	0.0456	0.0002

Best results with classification error < 5%

Fig. 14. Error in classification with different training datasets

that this training set covers the full range of temporal output values for the sensor patch and thus is effective in classification of the indentations. Due to the material properties of the sensor patch, such as relaxation behavior over time, significant variation of output values were obtained. These findings will lead to new calibration procedures accounting for the relaxation effects within the patch over time, and thus take into consideration the significant variation of the output values which is caused by the material properties of the sensor.

V. Conclusion

Adoption of sophisticated touch sensors on robotic hands has been hampered by the lack of fully flexible coatings that can easily be attached to existing hardware. Instead, touch sensors often rely on rigid parts or bulky processing equipment. In this paper, we presented a novel crossed-wire sensor design that aims to overcome these problems. It is fully flexible and works with only a limited set of connecting wires. It provides a soft coating for improving object grip. Spatial resolution can be easily varied to allow for different levels of accuracy, for example on the fingertips and the palm. Moreover, it can be produced in large sheets or easily stitched together from smaller ones.

Several prototypes have been manufactured and tested. As predicted in preliminary tests, the sensor patches exhibit good piezo-resistive behavior during mechanical loading. The investigation of the prototype patches on a specialised testbed to quantify the characteristics of the correlation between indentation and resulting electrical resistance revealed

a non-monotonic, velocity-dependent behavior. Simulation and SEM examination revealed that this behavior most likely results from the low adhesion between the matrix material and the cast-in wires. Therefore, future focus for the development of our tactile sensors we lay on the improvement of the adhesion between the basis material and the contacting wires, for example by using non-metal wires.

The conducted classification tests have shown that the realised spatial resolution of the taxels of 0.8 mm enables the reliable classification of very small objects in multiple contact scenarios. Experiments were performed for the center of the sensor patch and its four corners. Each corner position had a deviation of about 1.5 mm from the center position. It was shown, that the patch resolution enables classifying indentations at different positions correctly with an accuracy of about 98% using a basic 2-layer artificial neural network. The applied neural network was also successful in classifying single and multiple point indentations. Even multiple-contact-point indentations adjacent to each other and deviated by only 1.5 mm can efficiently be discriminated by the sensor prototype. Comparing the results to the human fingertip performance [15] we were able to achieve similar spatial resolution for our sensor prototype.

VI. Acknowledgments

The authors gratefully acknowledge the support of the colleagues at the DLR-Institute for Robotics and Mechatronics and at the Department and Chair for Medical Engineering of Technische Universität München. This work is supported by the FP6 EU project SENSOPAC (028056).

References

[1] S. Ando, H. Shinoda, A. Yonenaga, and J. Terao. Ultrasonic six-axis deformation sensing. *IEEE Transactions on Ultrasonics, Ferroelectrics and Frequency Control*, 48(4):1031–1045, 07 2001.

[2] Y. Boulenger, E. Kramer, H. Liu, N. Seitz, and G. Hirzinger. An intelligent linear actuator and its control system. In *Proceedings of the IEEE/ASME International Conference on Advanced Intelligent Mechatronics*, 2001.

[3] J. Butterfass, M. Grebenstein, H. Liu, and G. Hirzinger. Dlr-hand ii: Next generation of a dextrous robot hand. In *Proceedings of the IEEE Int. Conf. on Robotics and Automation*, 2003.

[4] J.J. Clark. A magnetic field based compliance matching sensor for high resolution, high compliance tactile sensing. In *Proceedings of the IEEE International Conference on Intelligent Robots and Systems*, 1988.

[5] Cabot Corporation, 2008. Two Seaport Lane, Suite 1300, Boston, MA 02210.

[6] R. S. Dahiya, G. Metta, M. Valle, and G. Sandini. Tactile sensing—from humans to humanoids. *IEEE T Robot*, 26(1):1–20, 2010.

[7] C. Borst et al., editor. *Rollin' Justin - Mobile platform with variable base*. Robotics and Automation, 2009. ICRA '09. IEEE International Conference on, May 2009.

[8] Battenfeld GmbH. Microsystem 50, 2008. Brüsseler Straße 13 D-53842 Troisdorf.

[9] Space Control GmbH. Ofts optical force torque sensor, 2008. Am Technologiepark 10, D-82229 Seefeld.

[10] D. Goger, N. Gorges, and H. Worn. Tactile sensing for an anthropomorphic robotic hand: Hardware and signal processing. In *Robotics and Automation, 2009. ICRA '09. IEEE International Conference on*, pages 895–901, May 2009.

[11] D. Gunji, Y. Mizoguchi, S. Teshigawara, Aiguo Ming, A. Namiki, M. Ishikawaand, and M. Shimojo. Grasping force control of multi-fingered robot hand based on slip detection using tactile sensor. In *Robotics and Automation, 2008. ICRA 2008. IEEE International Conference on*, pages 2605–2610, May 2008.

[12] J.-C. Huang. Carbon black filled conducting polymers and polymer blends. *Advances in Polymer Technology*, 21(4):299–313, 06 2002.

[13] M. Hussain, Y.-H. Choa, and K. Niihara. Conductive rubber materials for pressure sensors. *Journal of Material Science Letters*, (20):525–527, 09 2001.

[14] ANSYS Inc. Ansys smart engineering simulation, 2008. Southpointe, 275 Technology Drive, Canonsburg, PA 15317.

[15] Per Jenmalm. *Dexterous Manipulation in Humans: Use of Visual and Tactile Information about Object Shape in Control of Fingertip Actions*. PhD thesis, UmeåUniversity, Sweden, 2000.

[16] K. Kamiyama, H. Kajimoto, N. Kawakami, and S. Tachi. Evaluation of a vision-based tactile sensor. In *Proceedings of the IEEE International Conference on Robotics and Automation*, 2004.

[17] A. Katada, Y. F. Buys, Y. Tominaga, S. Asai, and M. Sumita. Resistivity control in the semiconductive region for carbon-black-filled polymer composites. *Colloid Polymer Science*, 283:367374, 2005.

[18] H. Kawasaki, T. Komatsu, and K. Uchiyama. Dexterous anthropomorphic robot hand with distributed tactile sensor: Gifu hand ii. *IEEE/ASME Transactions on Mechatronics*, 7(3):296–303, 2002.

[19] C.-T. Ko, S.-H. Tseng, and M. S.-C. Lu. A cmos micromachined capacitive tactile sensor with high-frequency output. *Journal of Microelectromechanical Systems*, 15(6):1708–1714, 12 2006.

[20] E.S. Kolesar and C.S. Dyson. Object imaging with a piezoelectric robotic tactile sensor. *Journal of Microelectromechanical Systems*, 4(2):87–96, 06 1995.

[21] Hian Kai Kwa, J.H. Noorden, M. Missel, T. Craig, J.E. Pratt, and P.D. Neuhaus. Development of the ihmc mobility assist exoskeleton. In *Robotics and Automation, 2009. ICRA '09. IEEE International Conference on*, pages 2556–2562, May 2009.

[22] S.B. Lang and S. Muensit. Review of some lesser-known applications of piezoelectric and pyroelectric polymers. *Journal of Applied Physics A*, 85:125134, 2006.

[23] M.H. Lee and H.R. Nicholls. Tactile sensing for mechatronics - a state of the art survey. *Mechatronics*, 9:1–31, 1999.

[24] A. Maaroufi, K. Haboubi, A. El Amarti, and F. Carmona. Electrical resistivity of polymeric matrix loaded with nickel and cobalt powders. *Journal of Material Science*, 39:265 270, 2004.

[25] A.M. Okamura, N. Smaby, and M.R. Cutkosky. An overview of dexterous manipulation. In *Proceedings of the IEEE International Conference on Robotics and Automation*, 2000.

[26] D. De Rossi, F. Carpi, and E.P. Scilingo. Polymer based interfaces as bioinspired smart skins. *Advances in Colloid and Interface Science*, 116:165–178, 2005.

[27] K.P. Sau and D. Khastgir T.K. Chaki. Conductive rubber composites from different blends of ethylenepropylenediene rubber and nitrile rubber. *Journal of Material Science*, 32:5717–5724, 1997.

[28] R. Struempler and J. Glatz-Reichenbach. Feature article - conducting polymer composites. *Journal of Electroceramics*, 3/4:329–346, 1999.

[29] Iwata H. Sugano S. Sugaiwa, T. Shock absorbing skin design for human-symbiotic robot at the worst case collision. pages 481–486, 2008.

[30] T. Kishida T. Kawanami Y. Shimizu S. Iribe M. Fukushima T. Fujita M. Takahashi, T. Tsuboi. Adaptive grasping by multi fingered hand with tactile sensor based on robust force and position control. In *Robotics and Automation, 2008. ICRA 2008. IEEE International Conference on*, May 2008.

[31] KRAIBURG TPE GmbH und Co. KG, 2008. Friedrich-Schmidt-Strasse 2, 84478 Waldkraiburg, Germany.

[32] K. Weißand H. Wörn. The working principle of resistive tactile sensor cells. In *Proceedings of the IEEE International Conference on Mechatronics and Automation 2005*, 2005.

[33] V. Zucolotto, J. Avlyanov, and L.H.C. Mattoso. Elastomeric conductive composites based on conducting polymermodified carbon black. *Polymer Composites*, 25(6):617–621, 12 2004.